

Ultrafast control over chiral sum-frequency generation

Josh Vogwell¹, Laura Rego^{1,2}, Olga Smirnova^{3,4}, and David Ayuso^{1,3*}

¹*Department of Physics, Imperial College London, SW7 2AZ London, United Kingdom*

²*University of Salamanca, 37008 Salamanca, Spain*

³*Max-Born-Institut, Max-Born-Str. 2A, 12489 Berlin, Germany*

⁴*Technische Universität Berlin, 10623 Berlin, Germany*

E-mail: d.ayuso@imperial.ac.uk

Abstract

We introduce an ultrafast all-optical approach for efficient chiral recognition which relies on the interference between two low-order nonlinear processes which are ubiquitous in nonlinear optics: sum-frequency generation and third-harmonic generation. In contrast to traditional sum-frequency generation, our approach encodes the medium's handedness in the *intensity* of the emitted harmonic signal, rather than in its *phase*, and it enables full control over the enantiosensitive response. We show how, by sculpting the sub-optical-cycle oscillations of the driving laser field, we can force one molecular enantiomer to emit bright light while its mirror twin remains dark, thus reaching the ultimate efficiency limit of chiral sensitivity via low-order nonlinear light-matter interactions. Our work paves the way for ultrafast and highly efficient imaging and control of the chiral electronic clouds of chiral molecules using lasers with moderate intensities, in all states of matter: from gases to liquids to solids, with molecular specificity and on ultrafast timescales.

Introduction

Chirality is a universal type of asymmetry that naturally arises in molecules, optical fields, viruses, or even galaxies. Just like a chiral glove would either fit our left or right hand, but not both, the two non-superimposable mirror-reflected versions of a chiral molecule (enantiomers) can behave very differently when they interact with another chiral entity, e.g. another chiral molecule. Since the majority of molecules supporting biological life are chiral, methods for detecting, quantifying and manipulating molecular chirality are of great importance and interest, particularly in biochemical and pharmaceutical contexts.

Traditional chiroptical methods¹⁻⁴ rely on weak linear effects which arise beyond the electric-dipole approximation, posing significant limitations for detecting dilute samples and ultrafast spectroscopy.⁵ This challenge⁶ can be addressed by developing and applying approaches which rely exclusively on the molecular response to the local polarisation of the electric-field vector of an electromagnetic wave.⁶⁻⁴⁷ One strategy is to record the forward-backward asymmetry in the photo-electron angular distributions upon ionisation with circularly polarised light.⁸⁻²¹ This method, originally proposed⁸ and implemented⁹⁻¹³ in the *linear* regime, has been extended to the *nonlinear*¹³⁻²⁵ (multi-photon) regime, where the use of two-color light pulses enables unique opportunities for coherent control,²²⁻²⁵ and has also been recently observed in anions.⁴⁸

The nonlinear regime of purely electric-dipole light-matter interactions also enables efficient all-optical chiral spectroscopy,³³⁻⁴⁷ and the same principle can be applied to microwave fields,²⁸⁻³² as predicted by Kral, Shapiro and coworkers^{49,50} and reformulated for molecular rotations by several groups.^{51,52} Chiral sum-frequency generation³³⁻³⁹ (SFG) is a well established method for chiral recognition. It requires two incident laser beams with frequencies $\omega_1 \neq \omega_2$ propagating in different directions, with wave vectors $\hat{\mathbf{k}}_1$ and $\hat{\mathbf{k}}_2$, and polarisation $\hat{\mathbf{e}}_1$ and $\hat{\mathbf{e}}_2$. The incident fields drive a second-order response in the medium at frequency $\omega_3 = \omega_1 + \omega_2$ with polarisation $\hat{\mathbf{e}}_3 = \hat{\mathbf{e}}_1 \times \hat{\mathbf{e}}_2$, which leads to emission of light at this frequency in the direction of $\hat{\mathbf{k}}_3 = \hat{\mathbf{k}}_1 + \hat{\mathbf{k}}_2$. SFG is strictly forbidden in the bulk of isotropic

media, such as randomly oriented molecules, unless they are chiral. Since it is driven by purely electric-dipole interactions, the induced signals can be strong if ω_3 is close to resonance.³⁵ However, the intensity of SFG is not enantiosensitive – the molecular handedness remains hidden in the phase of the emitted radiation.

To measure the phase of SFG, and thus the medium’s handedness, one can make it interfere with a reference signal using a local oscillator.³⁹ This achiral reference can also be generated from the chiral sample itself, making the near-field intensity enantiosensitive. To this end, one can take advantage of magnetic interactions,³⁴ or use a constant electric field,³⁷ although these strategies offer limited enantiosensitivity and opportunities for control.

Here we introduce an all-optical approach for efficient chiral discrimination that relies on the interference between two low-order nonlinear processes: chiral sum-frequency generation and achiral third-harmonic generation. We show how, by sculpting the sub-cycle oscillations of the laser’s electric field vector, we can control the ultrafast optical response of the molecules in a highly enantiosensitive manner: quenching the low-order nonlinear response of one molecular enantiomer while maximising it in its mirror twin. This work shows that high enantiosensitivity is not limited to highly non-linear processes:^{40–46} it also be achieved in the perturbative regime.

Results and discussion

Chiral sum-frequency generation (SFG) can be efficiently driven by any combination of frequencies $\omega_1 \neq \omega_2$, as long as $\omega_3 = \omega_1 + \omega_2$ is close to resonance.³⁵ Let us impose $\omega_2 = 2\omega_1$, and thus $\omega_3 = 3\omega$, with $\omega = \omega_1$ being the fundamental frequency, and consider the next-order nonlinear process: third-harmonic generation (THG). The medium can efficiently absorb 3 photons of frequency ω from the first beam, still at relatively low laser intensities, which leads to achiral polarization¹ at frequency 3ω . Can this achiral response of the molecule

¹By achiral we mean that the induced polarization has identical amplitude and phase in opposite molecular enantiomers

interfere with the sum-frequency response to produce an enantiosensitive interference? Unfortunately, momentum conservation dictates that, while the SFG and THG signals have the same frequency, they are emitted in different directions. Indeed, the THG signal co-propagates with the ω beam, as $\mathbf{k}_{\text{THG}} = 3\mathbf{k}_\omega$, whereas the SFG signal is emitted in between the two driving beams, because $\mathbf{k}_{\text{SFG}} = \mathbf{k}_\omega + \mathbf{k}_{2\omega}$. In the following, we show how, a relatively simple modification of the original SFG setup, allows us to overcome this limitation.

The proposed optical setup combines a linearly polarised beam with frequency ω and a second beam that carries cross-polarised ω and 2ω frequencies. The ω components are polarised in the plane of propagation, whereas the 2ω component is polarised orthogonal to this plane, see Fig. 1a. The laser field can be written as:

$$\mathbf{E} = \Re\{\mathbf{E}^{(1)} + \mathbf{E}^{(2)}\}, \quad (1)$$

$$\mathbf{E}^{(1)} = E_\omega^{(1)} e^{-i\omega t + i\mathbf{k}_1 \cdot \mathbf{r}} \hat{\mathbf{e}}_1, \quad (2)$$

$$\mathbf{E}^{(2)} = E_\omega^{(2)} e^{-i\omega t + i\mathbf{k}_2 \cdot \mathbf{r}} \hat{\mathbf{e}}_2 + E_{2\omega}^{(2)} e^{-2i\omega t - i\phi_{2\omega} + 2i\mathbf{k}_2 \cdot \mathbf{r}} \hat{\mathbf{e}}_3, \quad (3)$$

where $E_\omega^{(1)}$, $E_\omega^{(2)}$ and $E_{2\omega}^{(2)}$ are the electric-field amplitudes including the temporal and spatial Gaussian envelopes, and $\phi_{2\omega}$ is the two-colour phase delay in the second beam.

In our setup (Fig. 1a), we set the ratio between the two input frequencies to $\omega_2/\omega_1 = 2$, and add the fundamental ω frequency to the second beam. These two key features determine a fundamental difference in the properties of the created field with respect to traditional SFG configurations. In traditional SFG setups, the polarization of the electric-field vector is confined to a plane, and therefore achiral within the electric-dipole approximation. In our setup, the combination of the two beams creates a locally chiral field: the polarization of the electric-field vector draws a (three-dimensional) chiral trajectory in time.⁴¹

The generated locally chiral field can drive a strongly enantiosensitive response in a medium of randomly oriented chiral molecules via interference between SFG and THG, see Fig. 1b. The SFG pathway is as in traditional SFG implementations, see Fig. 1c (left).

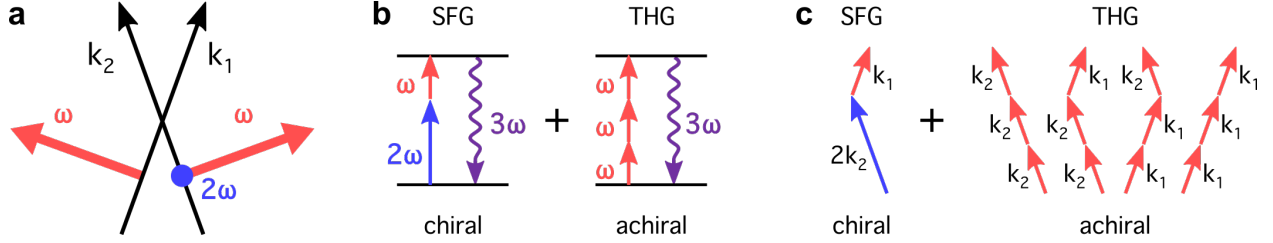


Figure 1: **enantiosensitive SFG**. **a**, The proposed optical setup combines a linearly polarised beam with frequency ω and a second beam that carries cross-polarised ω and 2ω frequencies. The ω frequency components are polarised in the plane of propagation, the 2ω component is polarised orthogonal to this plane. **b**, Multiphoton pathways describing chiral SFG (left) and achiral THG (right). The induced polarisation associated with SFG has the same amplitude and opposite phase in opposite molecular enantiomers, $P_{SFG}^L = -P_{SFG}^R$, whereas the polarisation associated with THG is identical, $P_{THG}^L = P_{THG}^R$. **c**, Multiphoton diagrams describing momentum conservation in SFG (left) and THG (right).

However, by adding the ω frequency to the second beam, we open new THG pathways, see Fig. 1c (right). The medium can now absorb the three ω photons from the same beam, or two photons from one beam and one from the other, giving rise to emission of achiral THG in four different directions. Importantly, one of these pathways, the one involving absorption of one photon from the first beam and two photons from the second beam, leads to achiral THG emission exactly in the same direction as the chiral SFG signal (Fig. 1c). The two contributions can now interfere, making the intensity of emission strongly enantiosensitive.

To demonstrate our proposal, we have performed state-of-the-art numerical simulations in randomly oriented propylene oxide molecules, see Methods. We have considered the following laser parameters: intensity of the ω field in the first and second beams $I_{\omega}^{(1)} = I_{\omega}^{(2)} = 3 \cdot 10^{12}$ W/cm², intensity of the 2ω component $I_{2\omega}^{(2)} = 7 \cdot 10^{11}$ W/cm², pulse duration 7 fs, and opening angle $2\alpha = 50^\circ$. Fig. 2a,b shows the intensity of the two contributions to emission at frequency 3ω in the far field (SFG and THG). As already anticipated, the chiral SFG contribution is emitted at a divergence angle $\arcsin(\sin(\alpha)/3) = 8.1^\circ$ (Fig. 1c, left), whereas the achiral THG profile shows 4 peaks, at angles -25.0° , -8.1° , 8.1° and 25.0° , corresponding to the 4 possible k -vectors' combinations (Fig. 1c, right).

The intensity profiles of the SFG and THG contributions are, individually, not enan-

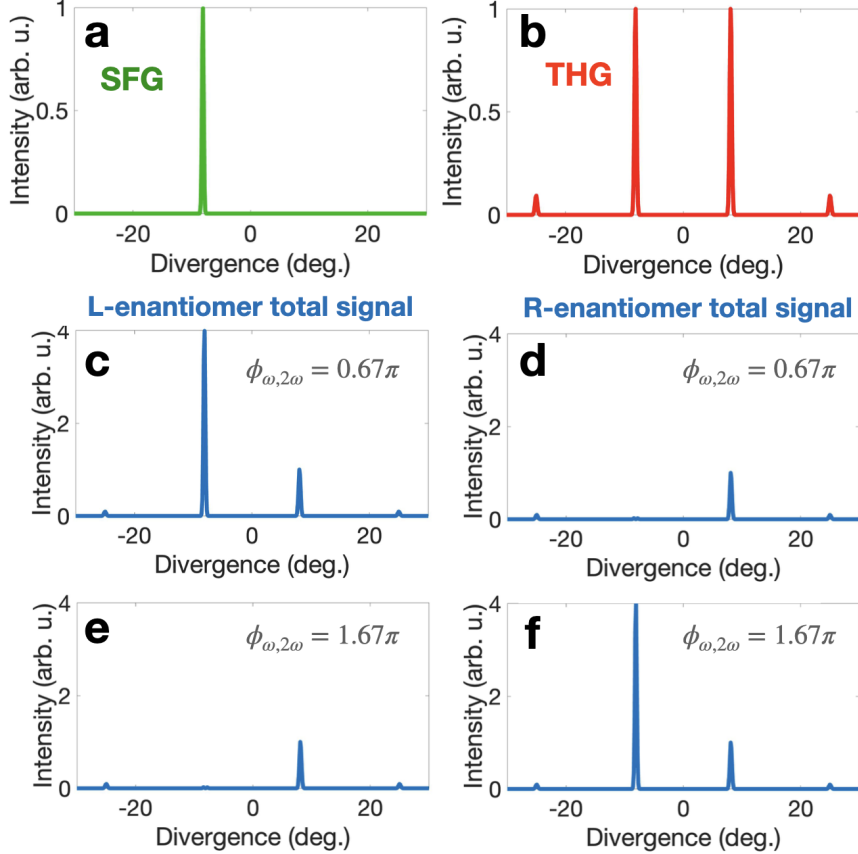


Figure 2: **enantiosensitive SFG in propylene oxide.** **a,b**, Intensity at frequency 3ω in the far field associated with chiral SFG (**a**) and achiral THG (**b**). **c-f** Total intensity emitted from L (**c,e**) and R (**d,f**), resulting from adding the chiral SFG (**a**) and achiral THG (**b**) contributions, for $\phi_{\omega,2\omega} = 0.67\pi$ (**c,d**) and $\phi_{\omega,2\omega} = 1.67\pi$ (**e,f**). Laser parameters: $I_{\omega}^{(1)} = I_{\omega}^{(2)} = 3 \cdot 10^{12} \text{ W/cm}^2$, $I_{2\omega}^{(2)} = 7 \cdot 10^{11} \text{ W/cm}^2$, pulse duration 7 fs, and opening angle $2\alpha = 50^\circ$.

tiosensitive (Fig. 2a,b). However, since the SFG contribution is out of phase in opposite molecular enantiomers, the total intensity of emission, resulting from adding the two contributions, becomes strongly enantiosensitive, see Fig. 2c-f. We have tuned the amplitude of the 2ω component of the driving field so the SFG contribution and the THG contribution at emission angle -8.1° have equal amplitude. Then, we adjusting the two-colour phase delay in the driving field, we control the phase of SFG, achieving full control over the enantiosensitive interference, and thus over the intensity of emission at frequency 3ω . For $\phi_{2\omega} = 0.67\pi$, the SFG and THG contributions interfere constructively in the left-handed molecules (Fig. 2c) and destructively in the right-handed molecules (Fig. 2d). Changing the two-colour delay by

π , i.e. setting $\phi_{2\omega} = 1.67\pi$, changes the phase of the SFG contribution by π , leading to the opposite effect: suppression from the left-handed molecules (Fig. 2e) and strong emission from the right-handed molecules (Fig. 2f).

Fig. 3 shows how we can fully control the intensity of emission at angle -8.1° in a highly enantiosensitive manner. Indeed, because the polarisation associated with SFG is out of phase in opposite enantiomers, the values of the two-colour delay that maximise and quench emission from the L (Fig. 3a) and R (Fig. 3b) enantiomers are shifted by π . Note that the specific values of the two-colour delay that optimise the enantiosensitive interference depend on the relative phase between the SFG and THG contributions to light-induced polarisation, which record the anisotropy of the chiral molecular potential and thus are molecule-specific quantities.

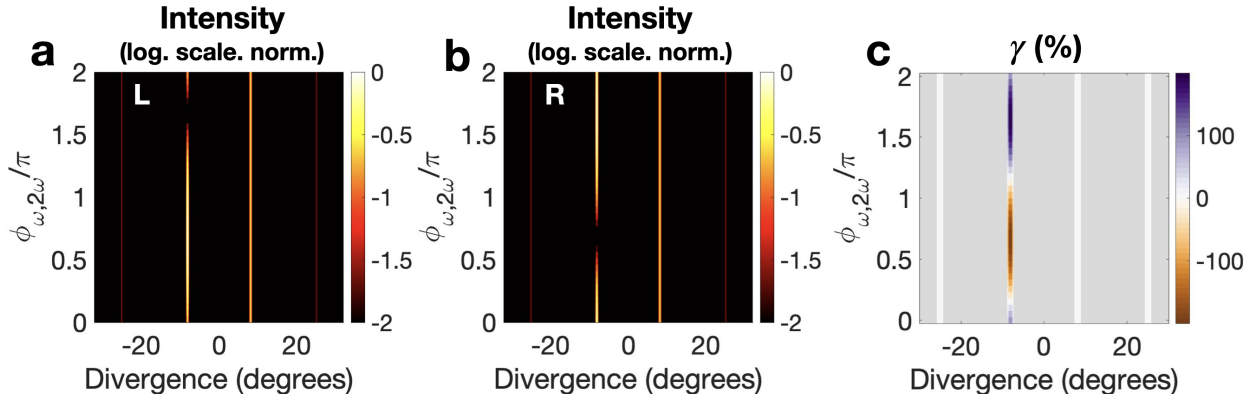


Figure 3: **enantiosensitive control of SFG.** **a,b**, Intensity at frequency 3ω emitted from left-handed (**a**) and right-handed (**b**) propylene oxide as a function of the divergence angle and the two-colour phase delay. **c**, Dissymmetry factor $\gamma = 2(I_L - I_R)/(I_L + I_R)$. Grey color indicates no intensity of emission. See caption of Fig. for laser parameters.

To quantify the degree of enantiosensitivity in the nonlinear optical response, we use a standard definition of the dissymmetry factor, $\gamma = \frac{I_L - I_R}{(I_L + I_R)/2}$. As shown in Fig. 3c, γ reaches the limits of $\pm 200\%$. That is, we can maximise emission from the left-handed molecules and fully quench it in the right-handed molecules ($\gamma = 200\%$), or vice versa ($\gamma = -200\%$), by adjusting the two-colour phase delay in the second beam. Indeed, because the two-colour delay defines the local handedness of the locally chiral field, it controls the enantiosensitive

response of the chiral molecules.

Note that, while the intensity of emission at angle -8.1° is strongly enantiosensitive and can be fully controlled, the peak at 8.1° is completely independent on both the molecular handedness and the two-colour delay. This is due to the different phase matching conditions for SFG and THG, as can be understood in terms of conservation of momentum (Fig. 1), which dictate that the peak at 8.1° is solely due to THG. Thus, this peak constitutes a constant reference which can be used for calibration purposes and for reducing the noise in experimental measures.

Conclusions

Our proposal constitutes a simple, yet highly efficient, all-optical approach for chiral discrimination that relies on the interference between low-order nonlinear phenomena (SFG and THG) which are ubiquitous in nonlinear optics. They have both been widely recorded in chiral and achiral media, in isotropic and anisotropic samples, and in the gas, liquid, and solid phases of matter. Yet, despite the general importance of chiral molecules, to the best of our knowledge, these two phenomena had not been combined to achieve efficient chiral discrimination.

Our approach takes advantage of the tremendous capabilities of modern optical technology for sculpting the polarization of light with sub-optical-cycle temporal resolution. Indeed, by controlling the two-colour delay in the proposed optical setup, we can tailor the chirality of the driving field in order to maximise the nonlinear response of a selected molecular enantiomer while suppressing it in its mirror twin.

The possibility of driving strongly enantiosensitive interactions via low-order nonlinear processes creates tremendous opportunities for imaging and controlling molecular chirality on ultrafast timescales using laser fields with gentle intensities, as well as for developing enantiosensitive optical traps and tweezers.

Acknowledgments

We acknowledge enlightening discussions with Misha Ivanov, Andrés Ordoñez, Rose Picciuto, Mary Matthews and Jon Marangos. L. R. acknowledges financial support from the European Union-NextGenerationEU and the Spanish Ministry of Universities via her Margarita Salas Fellowship through the University of Salamanca; J. V., L. R. and D. A. acknowledge funding from the Royal Society URF\R1\201333 and URF\ERE\210358. Funded by the European Union (ERC, ULISSES, 101054696). Views and opinions expressed are however those of the author(s) only and do not necessarily reflect those of the European Union or the European Research Council. Neither the European Union nor the granting authority can be held responsible for them.

Methods

Single-molecule response of randomly oriented propylene oxide

The ultrafast electronic response randomly oriented propylene oxide to the proposed driving field was evaluated using real-time time-dependent density functional (TDDFT) theory in Octopus.⁵³⁻⁵⁶ We used the local density approximation⁵⁷⁻⁵⁹ to account for electronic exchange and correlation effects, together with the averaged density self-interaction correction.⁶⁰ The 1s orbitals of the carbon and oxygen atoms were described by pseudopotentials. We expanded the Kohn-Sham orbitals and the electron density onto a spherical basis set of radius $R = 41.9$ a.u., with $\Delta x = 0.4$ a.u. of spacing between adjacent grid points, and used a complex absorbing potential of width 20 a.u. and height -0.2 a.u. to avoid unphysical reflection effects. In our TDDFT simulations, we used a two-colour cross-polarised driving field,

$$\mathbf{E}_0(t) = a(t)[E_\omega^{(0)} \cos(\omega t)\hat{\mathbf{x}} + E_{2\omega}^{(0)} \cos(2\omega t)\hat{\mathbf{z}}], \quad (4)$$

where $E_\omega^{(0)} = E_{2\omega}^{(0)} = 0.00534$ a.u. are the electric-field amplitudes, $\omega = 0.126$ a.u. is the fundamental frequency, and $a(t)$ is sine-squared flat-top envelope of 8 laser cycles of the fundamental frequency, with 2 cycles to rise up, 4 cycles of constant amplitude, and 2 cycles to go down.

We run TDDFT simulations for 208 different molecular orientations to evaluate the induced polarisation in the randomly oriented ensemble:

$$\mathbf{P}_0 = \frac{1}{8\pi^2} \int_0^{2\pi} \int_0^\pi \int_0^{2\pi} \mathbf{P}_{\phi\theta\chi} \sin(\theta) d\phi d\theta d\chi, \quad (5)$$

where ϕ , θ and χ are the Euler angles, and $\mathbf{P}_{\phi\theta\chi}$ is the polarisation induced in a particular molecular orientation in the laboratory frame. We used the Lebedev quadrature⁶¹ of order 7 to integrate over ϕ and θ , thus using 26 points to sample the two angles, and the trapezoid method to integrate numerically over χ , using 8 angular points.

Laser field in the interaction region

The laser field was modelled using Eqs. 1-3 of the main text, with $\mathbf{k}_{1,2} = \frac{2\pi}{\lambda}[\pm \sin(\alpha)\hat{\mathbf{x}} + \cos(\alpha)\hat{\mathbf{y}}]$, where $\lambda = 362$ nm is the fundamental wavelength. The two beams propagate in the xy plane, at angles $\pm\alpha$ with respect to the y axis. We assume a thin medium, which could be realised using a flat liquid microjet,^{62?} and thus neglect the spatial modulation of the field properties along the propagation direction, and set the position of the thin sample at $y = 0$. Setting intensity of the ω frequency component to be the same in the two beams, the total electric-field vector of the laser at $y = z = 0$ can be written as

$$\mathbf{E}(x, t) = a(t)[E_x(x) \cos(\omega t)\hat{\mathbf{x}} + E_y(x) \sin(\omega t)\hat{\mathbf{y}} + E_z(x) \cos(2\omega t + \phi(x))\hat{\mathbf{z}}], \quad (6)$$

with

$$E_x(x) = 2E_\omega \cos(\alpha) \cos(k \sin \alpha x) e^{-x^2/w^2}, \quad (7)$$

$$E_y(x) = 2E_\omega \sin(\alpha) \sin(k \sin \alpha x) e^{-x^2/w^2}, \quad (8)$$

$$E_z(x) = E_{2\omega} e^{-x^2/w^2}, \quad (9)$$

$$\phi(x) = \phi_{2\omega} + 2k \sin(\alpha) x, \quad (10)$$

where E_ω and $E_{2\omega}$ are the electric-field amplitudes, w is the waist of the Gaussian beams, and $\phi_{2\omega}$ is the two-colour phase delay in the second beam.

Nonlinear response in the near field

The enantiosensitive response of the molecules at frequency 3ω results from the interference between contributions to light-induced polarisation: chiral sum-frequency generation (SFG) and achiral third-harmonic generation (THG), see Fig. 1 of the main text. The SFG and THG contributions were obtained by projecting the induced polarisation in the frequency domain \mathbf{P}_0 over the x and y axis, $\mathbf{P}_0^{\text{THG}} = \mathbf{P}_0(3\omega) \cdot \hat{\mathbf{x}}$ and $\mathbf{P}_0^{\text{SFG}} = \mathbf{P}_0(3\omega) \cdot \hat{\mathbf{y}}$.

Note that this procedure neglects the contribution of the y component of the electric-field vector to both THG and SFG, which reduces significantly the computational cost of the simulations. As a result, $\mathbf{P}_0^{\text{THG}}$ and $\mathbf{P}_0^{\text{SFG}}$ are linearly polarised along x and y , respectively, and not elliptically polarised in the xy plane. Including the y component of the electric-field vector in the simulations would make both \mathbf{P}^{THG} and \mathbf{P}^{SFG} elliptically polarised in the xy plane, but it would not lead to significant changes in the results presented in the main text.

To model the nonlinear response of the molecules across the interaction region, we assumed that the induced polarisation depends on the field amplitudes according to the number

of absorbed photons (see Fig. 1 of the main text),

$$\mathbf{P}^{\text{THG}}(x) = \mathbf{P}_0^{\text{THG}} \left(\frac{E_x(x)}{E_\omega^{(0)}} \right)^3, \quad (11)$$

$$\mathbf{P}^{\text{SFG}}(x) = \mathbf{P}_0^{\text{SFG}} \frac{E_x(x)}{E_\omega^{(0)}} \frac{E_z(x)}{E_{2\omega}^{(0)}} e^{i\phi(x)}, \quad (12)$$

where $E_\omega^{(0)}$ and $E_{2\omega}^{(0)}$ are the electric-field amplitudes used in the TDDFT simulations (Eq. 4), and E_x , E_z and ϕ are the field-amplitudes and phase delay across the transverse coordinate x (Eq. 6). We performed calculations for the right handed enantiomer of propylene oxide, and the results for the left handed enantiomer were obtained using symmetry arguments.

Enantiosensitive intensity in the far field

The far-field image was evaluated using Fraunhofer diffraction:

$$\mathbf{E}(\kappa) \propto 9\omega^2 \int_{-\infty}^{\infty} \mathbf{P}_\perp(x) e^{-iKx} dx, \quad (13)$$

where κ is the far-field angle (divergence), \mathbf{P}_\perp is the projection of the total polarisation at frequency 3ω , $\mathbf{P} = \mathbf{P}^{\text{THG}} + \mathbf{P}^{\text{SFG}}$ (Eqs. 11 and 12), onto the plane that is orthogonal to the propagation direction $\hat{\mathbf{k}} = \cos(\kappa)\hat{\mathbf{x}} + \sin(\kappa)\hat{\mathbf{y}}$, and $K = \frac{3\omega}{c} \sin(\kappa)$, with ω being the fundamental frequency, and c being the speed of light in vacuum.

References

- (1) Berova, N.; Bari, L. D.; Pescitelli, G. Application of electronic circular dichroism in configurational and conformational analysis of organic compounds. *Chem. Soc. Rev.* **2007**, *36*, 914–931.
- (2) Nafie, L. A.; Keiderling, T. A.; Stephens, P. J. Vibrational circular dichroism. *Journal of the American Chemical Society* **1976**, *98*, 2715–2723.

- (3) Schellman, J. A. Circular dichroism and optical rotation. *Chemical Reviews* **1975**, *75*, 323–331.
- (4) Polavarapu, P. L.; Chakraborty, D. K. Absolute Stereochemistry of Chiral Molecules from ab Initio Theoretical and Experimental Molecular Optical Rotations. *Journal of the American Chemical Society* **1998**, *120*, 6160–6164.
- (5) Oppermann, M.; Spekowius, J.; Bauer, B.; Pfister, R.; Chergui, M.; Helbing, J. Broad-Band Ultraviolet CD Spectroscopy of Ultrafast Peptide Backbone Conformational Dynamics. *The Journal of Physical Chemistry Letters* **2019**, *10*, 2700–2705.
- (6) Ayuso, D.; Ordonez, A. F.; Smirnova, O. Ultrafast chirality: the road to efficient chiral measurements. *Phys. Chem. Chem. Phys.* **2022**, *24*, 26962–26991.
- (7) Ordonez, A. F.; Smirnova, O. Generalized perspective on chiral measurements without magnetic interactions. *Phys. Rev. A* **2018**, *98*, 063428.
- (8) Ritchie, B. Theory of the angular distribution of photoelectrons ejected from optically active molecules and molecular negative ions. *Phys. Rev. A* **1976**, *13*, 1411–1415.
- (9) Powis, I. Photoelectron circular dichroism of the randomly oriented chiral molecules glyceraldehyde and lactic acid. *The Journal of Chemical Physics* **2000**, *112*, 301–310.
- (10) Böwering, N.; Lischke, T.; Schmidtke, B.; Müller, N.; Khalil, T.; Heinzmann, U. Asymmetry in Photoelectron Emission from Chiral Molecules Induced by Circularly Polarized Light. *Phys. Rev. Lett.* **2001**, *86*, 1187–1190.
- (11) Garcia, G. A.; Nahon, L.; Lebech, M.; Houver, J.-C.; Doweck, D.; Powis, I. Circular dichroism in the photoelectron angular distribution from randomly oriented enantiomers of camphor. *The Journal of Chemical Physics* **2003**, *119*, 8781–8784.

- (12) Garcia, G. A.; Nahon, L.; Daly, S.; Powis, I. Vibrationally induced inversion of photoelectron forward-backward asymmetry in chiral molecule photoionization by circularly polarized light. *Nature Communications* **2013**, *4*, 2132.
- (13) Janssen, M. H. M.; Powis, I. Detecting chirality in molecules by imaging photoelectron circular dichroism. *Phys. Chem. Chem. Phys.* **2014**, *16*, 856–871.
- (14) Lux, C.; Wollenhaupt, M.; Bolze, T.; Liang, Q.; Köhler, J.; Sarpe, C.; Baumert, T. Circular Dichroism in the Photoelectron Angular Distributions of Camphor and Fenchone from Multiphoton Ionization with Femtosecond Laser Pulses. *Angewandte Chemie International Edition* **2012**, *51*, 5001–5005.
- (15) Lehmann, C. S.; Ram, N. B.; Powis, I.; Janssen, M. H. M. Imaging photoelectron circular dichroism of chiral molecules by femtosecond multiphoton coincidence detection. *The Journal of Chemical Physics* **2013**, *139*, 234307.
- (16) Lux, C.; Wollenhaupt, M.; Sarpe, C.; Baumert, T. Photoelectron Circular Dichroism of Bicyclic Ketones from Multiphoton Ionization with Femtosecond Laser Pulses. *ChemPhysChem* **2015**, *16*, 115–137.
- (17) Kastner, A.; Lux, C.; Ring, T.; Züllighoven, S.; Sarpe, C.; Senftleben, A.; Baumert, T. Enantiomeric Excess Sensitivity to Below One Percent by Using Femtosecond Photoelectron Circular Dichroism. *ChemPhysChem* **2016**, *17*, 1119–1122.
- (18) Comby, A.; Beaulieu, S.; Boggio-Pasqua, M.; Descamps, D.; Légaré, F.; Nahon, L.; Petit, S.; Pons, B.; Fabre, B.; Mairesse, Y.; Blanchet, V. Relaxation Dynamics in Photoexcited Chiral Molecules Studied by Time-Resolved Photoelectron Circular Dichroism: Toward Chiral Femtochemistry. *The Journal of Physical Chemistry Letters* **2016**, *7*, 4514–4519, PMID: 27786493.
- (19) Beaulieu, S.; Comby, A.; Fabre, B.; Descamps, D.; Ferré, A.; Garcia, G.; Généaux, R.; Légaré, F.; Nahon, L.; Petit, S.; Ruchon, T.; Pons, B.; Blanchet, V.; Mairesse, Y.

- Probing ultrafast dynamics of chiral molecules using time-resolved photoelectron circular dichroism. *Faraday Discuss.* **2016**, *194*, 325–348.
- (20) Comby, A.; Bloch, E.; Bond, C. M. M.; Descamps, D.; Miles, J.; Petit, S.; Rozen, S.; Greenwood, J. B.; Blanchet, V.; Mairesse, Y. Real-time determination of enantiomeric and isomeric content using photoelectron elliptical dichroism. *Nature Communications* **2018**, *9*, 5212.
- (21) Beaulieu, S. et al. Photoexcitation circular dichroism in chiral molecules. *Nature Physics* **2018**,
- (22) Demekhin, P. V.; Artemyev, A. N.; Kastner, A.; Baumert, T. Photoelectron Circular Dichroism with Two Overlapping Laser Pulses of Carrier Frequencies ω and 2ω Linearly Polarized in Two Mutually Orthogonal Directions. *Phys. Rev. Lett.* **2018**, *121*, 253201.
- (23) Goetz, R. E.; Koch, C. P.; Greenman, L. Quantum Control of Photoelectron Circular Dichroism. *Phys. Rev. Lett.* **2019**, *122*, 013204.
- (24) Rozen, S.; Comby, A.; Bloch, E.; Beauvarlet, S.; Descamps, D.; Fabre, B.; Petit, S.; Blanchet, V.; Pons, B.; Dudovich, N.; Mairesse, Y. Controlling Subcycle Optical Chirality in the Photoionization of Chiral Molecules. *Phys. Rev. X* **2019**, *9*, 031004.
- (25) Ordonez, A. F.; Smirnova, O. Disentangling enantiosensitivity from dichroism using bichromatic fields. *Phys. Chem. Chem. Phys.* **2022**, *24*, 7264–7273.
- (26) Yachmenev, A.; Onvlee, J.; Zak, E.; Owens, A.; Küpper, J. Field-Induced Diastereomers for Chiral Separation. *Phys. Rev. Lett.* **2019**, *123*, 243202.
- (27) Milner, A. A.; Fordyce, J. A. M.; MacPhail-Bartley, I.; Wasserman, W.; Milner, V.; Tutunnikov, I.; Averbukh, I. S. Controlled Enantioselective Orientation of Chiral Molecules with an Optical Centrifuge. *Phys. Rev. Lett.* **2019**, *122*, 223201.

- (28) Patterson, D.; Schnell, M.; Doyle, J. M. Enantiomer-specific detection of chiral molecules via microwave spectroscopy. *Nature* **2013**, *497*, 475–477.
- (29) Eibenberger, S.; Doyle, J.; Patterson, D. Enantiomer-Specific State Transfer of Chiral Molecules. *Phys. Rev. Lett.* **2017**, *118*, 123002.
- (30) Shubert, V. A.; Schmitz, D.; Pérez, C.; Medcraft, C.; Krin, A.; Domingos, S. R.; Patterson, D.; Schnell, M. Chiral Analysis Using Broadband Rotational Spectroscopy. *The Journal of Physical Chemistry Letters* **2016**, *7*, 341–350, PMID: 26745342.
- (31) Pérez, C.; Steber, A. L.; Domingos, S. R.; Krin, A.; Schmitz, D.; Schnell, M. Coherent Enantiomer-Selective Population Enrichment Using Tailored Microwave Fields. *Angewandte Chemie International Edition* **2017**, *56*, 12512–12517.
- (32) Lee, J.; Bischoff, J.; Hernandez-Castillo, A. O.; Sartakov, B.; Meijer, G.; Eibenberger-Arias, S. Quantitative Study of Enantiomer-Specific State Transfer. *Phys. Rev. Lett.* **2022**, *128*, 173001.
- (33) Fischer, P.; Wiersma, D. S.; Righini, R.; Champagne, B.; Buckingham, A. D. Three-Wave Mixing in Chiral Liquids. *Phys. Rev. Lett.* **2000**, *85*, 4253–4256.
- (34) Belkin, M. A.; Kulakov, T. A.; Ernst, K.-H.; Yan, L.; Shen, Y. R. Sum-Frequency Vibrational Spectroscopy on Chiral Liquids: A Novel Technique to Probe Molecular Chirality. *Phys. Rev. Lett.* **2000**, *85*, 4474–4477.
- (35) Belkin, M. A.; Han, S. H.; Wei, X.; Shen, Y. R. Sum-Frequency Generation in Chiral Liquids near Electronic Resonance. *Phys. Rev. Lett.* **2001**, *87*, 113001.
- (36) Fischer, P.; Beckwitt, K.; Wise, F.; Albrecht, A. The chiral specificity of sum-frequency generation in solutions. *Chemical Physics Letters* **2002**, *352*, 463–468.
- (37) Fischer, P.; Buckingham, A. D.; Beckwitt, K.; Wiersma, D. S.; Wise, F. W. New

- Electro-Optic Effect: Sum-Frequency Generation from Optically Active Liquids in the Presence of a dc Electric Field. *Phys. Rev. Lett.* **2003**, *91*, 173901.
- (38) Fischer, P.; Hache, F. Nonlinear optical spectroscopy of chiral molecules. *Chirality* **2005**, *17*, 421–437.
- (39) Okuno, M.; Ishibashi, T.-a. Bulk-or-interface assignment of heterodyne-detected chiral vibrational sum frequency generation signal by its polarization dependence. *The Journal of Chemical Physics* **2018**, *149*, 244703.
- (40) Neufeld, O.; Ayuso, D.; Decleva, P.; Ivanov, M. Y.; Smirnova, O.; Cohen, O. Ultra-sensitive Chiral Spectroscopy by Dynamical Symmetry Breaking in High Harmonic Generation. *Phys. Rev. X* **2019**, *9*, 031002.
- (41) Ayuso, D.; Neufeld, O.; Ordonez, A. F.; Decleva, P.; Lerner, G.; Cohen, O.; Ivanov, M.; Smirnova, O. Synthetic chiral light for efficient control of chiral light-matter interaction. *Nature Photonics* **2019**, *13*, 866–871.
- (42) Ayuso, D.; Ordonez, A. F.; Decleva, P.; Ivanov, M.; Smirnova, O. Enantio-sensitive unidirectional light bending. *Nature Communications* **2021**, *12*, 3951.
- (43) Ayuso, D.; Ordonez, A. F.; Ivanov, M.; Smirnova, O. Ultrafast optical rotation in chiral molecules with ultrashort and tightly focused beams. *Optica* **2021**, *8*, 1243–1246.
- (44) Ayuso, D. New opportunities for ultrafast and highly enantio-sensitive imaging of chiral nuclear dynamics enabled by synthetic chiral light. *Phys. Chem. Chem. Phys.* **2022**, *24*, 10193–10200.
- (45) Ayuso, D.; Ordonez, A. F.; Decleva, P.; Ivanov, M.; Smirnova, O. Strong chiral response in non-collinear high harmonic generation driven by purely electric-dipole interactions. *Opt. Express* **2022**, *30*, 4659–4667.

- (46) Rego, L.; Smirnova, O.; Ayuso, D. Tilting light's polarization plane to spatially separate the ultrafast nonlinear response of chiral molecules. *Nanophotonics* **2023**,
- (47) Khokhlova, M.; Pisanty, E.; Patchkovskii, S.; Smirnova, O.; Ivanov, M. Enantiosensitive steering of free-induction decay. *Science Advances* **2022**, *8*, eabq1962.
- (48) Triptow, J.; Fielicke, A.; Meijer, G.; Green, M. Imaging Photoelectron Circular Dichroism in the Detachment of Mass-Selected Chiral Anions. *Angewandte Chemie International Edition* **2023**, *62*, e202212020.
- (49) Král, P.; Shapiro, M. Cyclic Population Transfer in Quantum Systems with Broken Symmetry. *Phys. Rev. Lett.* **2001**, *87*, 183002.
- (50) Král, P.; Thanopoulos, I.; Shapiro, M.; Cohen, D. Two-Step Enantio-Selective Optical Switch. *Phys. Rev. Lett.* **2003**, *90*, 033001.
- (51) Lehmann, K. K. Influence of spatial degeneracy on rotational spectroscopy: Three-wave mixing and enantiomeric state separation of chiral molecules. *The Journal of Chemical Physics* **2018**, *149*, 094201.
- (52) Leibscher, M.; Giesen, T. F.; Koch, C. P. Principles of enantio-selective excitation in three-wave mixing spectroscopy of chiral molecules. *The Journal of chemical physics* **2019**, *151*, 014302.
- (53) Marques, M. A.; Castro, A.; Bertsch, G. F.; Rubio, A. octopus: a first-principles tool for excited electron-ion dynamics. *Computer Physics Communications* **2003**, *151*, 60–78.
- (54) Castro, A.; Appel, H.; Oliveira, M.; Rozzi, C. A.; Andrade, X.; Lorenzen, F.; Marques, M. A. L.; Gross, E. K. U.; Rubio, A. octopus: a tool for the application of time-dependent density functional theory. *physica status solidi (b)* **2006**, *243*, 2465–2488.

- (55) Andrade, X. et al. Real-space grids and the Octopus code as tools for the development of new simulation approaches for electronic systems. *Phys. Chem. Chem. Phys.* **2015**, *17*, 31371–31396.
- (56) Tancogne-Dejean, N. et al. Octopus, a computational framework for exploring light-driven phenomena and quantum dynamics in extended and finite systems. *The Journal of Chemical Physics* **2020**, *152*, 124119.
- (57) Dirac, P. A. M. Note on Exchange Phenomena in the Thomas Atom. *Mathematical Proceedings of the Cambridge Philosophical Society* **1930**, *26*, 376–385.
- (58) Bloch, F. Bemerkung zur Elektronentheorie des Ferromagnetismus und der elektrischen Leitfähigkeit. *Zeitschrift für Physik* **1929**, *57*, 545–555.
- (59) Perdew, J. P.; Zunger, A. Self-interaction correction to density-functional approximations for many-electron systems. *Phys. Rev. B* **1981**, *23*, 5048–5079.
- (60) Legrand, C.; Suraud, E.; Reinhard, P.-G. Comparison of self-interaction-corrections for metal clusters. *Journal of Physics B: Atomic, Molecular and Optical Physics* **2002**, *35*, 1115–1128.
- (61) Lebedev, V. I.; Laikov, D. N. A quadrature formula for the sphere of the 131st algebraic order of accuracy. *Doklady Mathematics* **1999**, *59*, 477–481.
- (62) Galinis, G.; Strucka, J.; Barnard, J. C. T.; Braun, A.; Smith, R. A.; Marangos, J. P. Micrometer-thickness liquid sheet jets flowing in vacuum. *Review of Scientific Instruments* **2017**, *88*, 083117.